Analysis of STAR ZDC SMD Data for Polarimetry

M.B. Bitters,[1,2] D.P. Grosnick,[1,2] D. Koetke,[1] J. Webb,[1] H. Spinka,[3] and B. Surrow[4]

[1] *Valparaiso University, Valparaiso, Indiana 46383*

[2] *Ball State University, Muncie, Indiana 47306*

[3] *Argonne National Laboratory, Argonne, Illinois 60439*

[4] *Massachusetts Institute of Technology, Cambridge, Massachusetts 02139*

(Dated: February 14, 2009)

Abstract

A spin physics program using the STAR detector at RHIC is underway that investigates the spin structure of the proton using polarized proton collisions at $\sqrt{s}$ = 200-500 GeV. The polarization of each beam is presently measured locally at STAR by the Beam-Beam Counters (BBC), but may give an insufficient polarization measurement due to a decreasing analyzing power at larger center-of-mass energies. Detectors located much further from the interaction region, such as the Zero Degree Calorimeters (ZDC), can measure the small-angle scattering of neutral particles and could serve as a local polarimeter at higher beam energies. Data from the Shower Maximum Detectors (SMD) of the ZDCs were analyzed to determine the feasibility of using these detectors as a local polarimeter. A seven sigma left-right physics asymmetry and an up-down physics asymmetry consistent with zero were measured from data taken in several dedicated runs in 2004. The physics asymmetry was also calculated as a function of azimuthal angle and displayed a sinusoidal pattern. These results demonstrate the capability of using the ZDC SMD as a local polarimeter for STAR.

I. INTRODUCTION

The main goal of the RHIC spin physics program is to more fully understand the spin structure of the proton, which may contain contributions from quarks, antiquarks, gluons, and orbital angular momentum. Detailed information from each contribution is limited or missing, and measurements from the collisions of polarized protons in the current program will provide needed data to help determine the origin of the proton's spin.

The RHIC facility is the first polarized collider, capable of producing transversely- or longitudinally-polarized proton beams with center-of-mass energies up to $\sqrt{s} = 500$ GeV. The absolute beam polarization is measured using the analyzing power of elastic p-p collisions in a polarized gas jet target, and is subsequently applied to determine the analyzing power for elastic p-C scattering measured in the Coulomb-nuclear interference (CNI) region. The calibrated p-C CNI polarimeters are then used to determine the beam polarization for each RHIC beam ("blue" and "yellow") several times during a RHIC store. Spin rotators are used to change the beam proton spin direction from transverse to longitudinal. To verify that the spin direction of the beam particles is the correct one at each large detector, a local polarimeter measures the beam polarization from the asymmetry of scattered particles in beam collisions. Currently, the Beam-Beam Counters (BBC) are used as the local polarimeter at STAR.

At higher beam energies, the BBCs may give an insufficient polarization measurement due to a decreasing analyzing power, and consequently limits its use as a local polarimeter. An independent experiment at RHIC [2] found a sizeable analyzing power for very forward scattered "neutrons", and the PHENIX collaboration used this information to construct a local polarimeter using their Zero Degree Calorimeters (ZDCs) [3]. The STAR ZDCs are located 18 m upstream and downstream of the interaction region and in back of beam-bending dipole magnets, and so they detect only very forward, neutral particles. Figure 1 displays the location of ZDCs with reference to the intersection point. The ZDCs have been primarily used as forward neutral detectors for the heavy-ion collisions.

In 2004, several dedicated data-gathering runs using polarized protons were taken that included information from the ZDCs. These data were analyzed to calculate an asymmetry from scattered neutral particles from polarized proton collisions at $\sqrt{s} = 200$ GeV. This report describes the analysis of data from the ZDC detectors during these runs. The ZDC

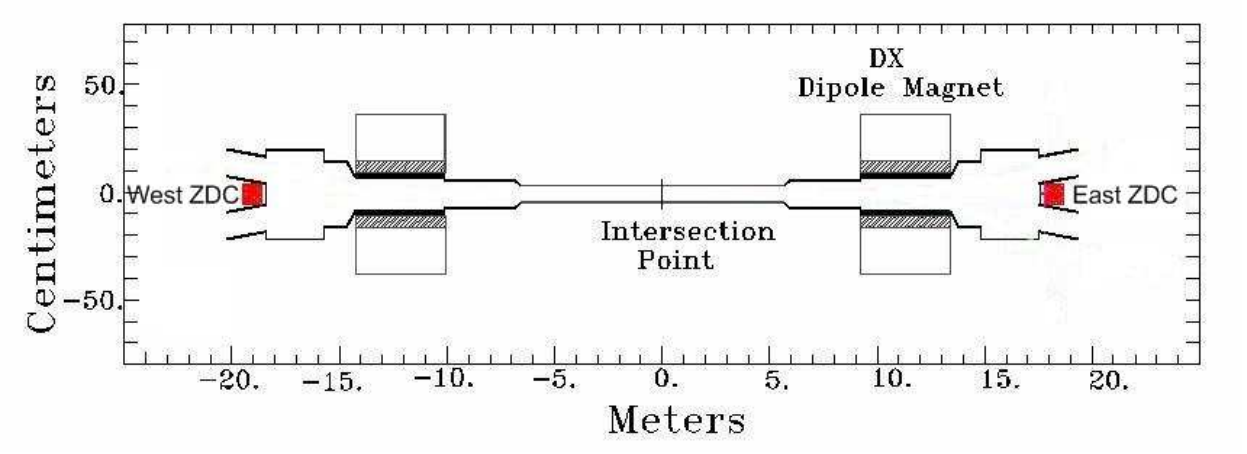

FIG. 1: Map of the beam lines around the intersection region. Note the large difference in scales where the horizontal distance is measured in meters and the vertical distance in centimeters. The location of each ZDC is shown at 18 m on either side, east and west, of the intersection point.

detector and hardware are described in Section II, the data analysis is given in Section III, details of the calculated asymmetries and results are provided in Section IV, and finally the conclusions are stated in Section V.

II. HARDWARE DESCRIPTION

The Zero Degree Calorimeters were designed to detect and measure the total energy of neutral particles emitted within a small angle of divergence from heavy-ion collisions (see, for example, Ref. [1]). These measurements can then be used to determine the beam luminosity. High-energy collisions of nuclei usually result in the emission or evaporation of neutral particles from both beam and target nuclei. These neutral particles diverge by less than 2 milliradians from the axis of the beam. Charged particles produced in this zero degree region are mainly swept away by beam-line magnets, and consequently deposit an insignificant amount of energy in the ZDCs compared to the beam-fragmentation neutral particles. It has been estimated (Ref. [2]) that these neutral particles consist mostly of neutrons, even though there may be a small contamination from K_L^0 particles and antineutrons.

Two ZDCs are located in the forward directions, 18 meters on either side of the intersection point, as shown in Figure 1. One ZDC is on the east side and the other is on the west side. There is limited space available between the beams at RHIC for the ZDC, so the

total width of the calorimeters is not more than 10 centimeters. A schematic of a ZDC is displayed in Figure 2. Each ZDC is composed of three identical modules (1.7 interaction lengths each) that contain a particle shower, and each module is tilted at a 45° angle relative to the beam. Many details of the ZDC design are described in Ref. [4] and summarized below.

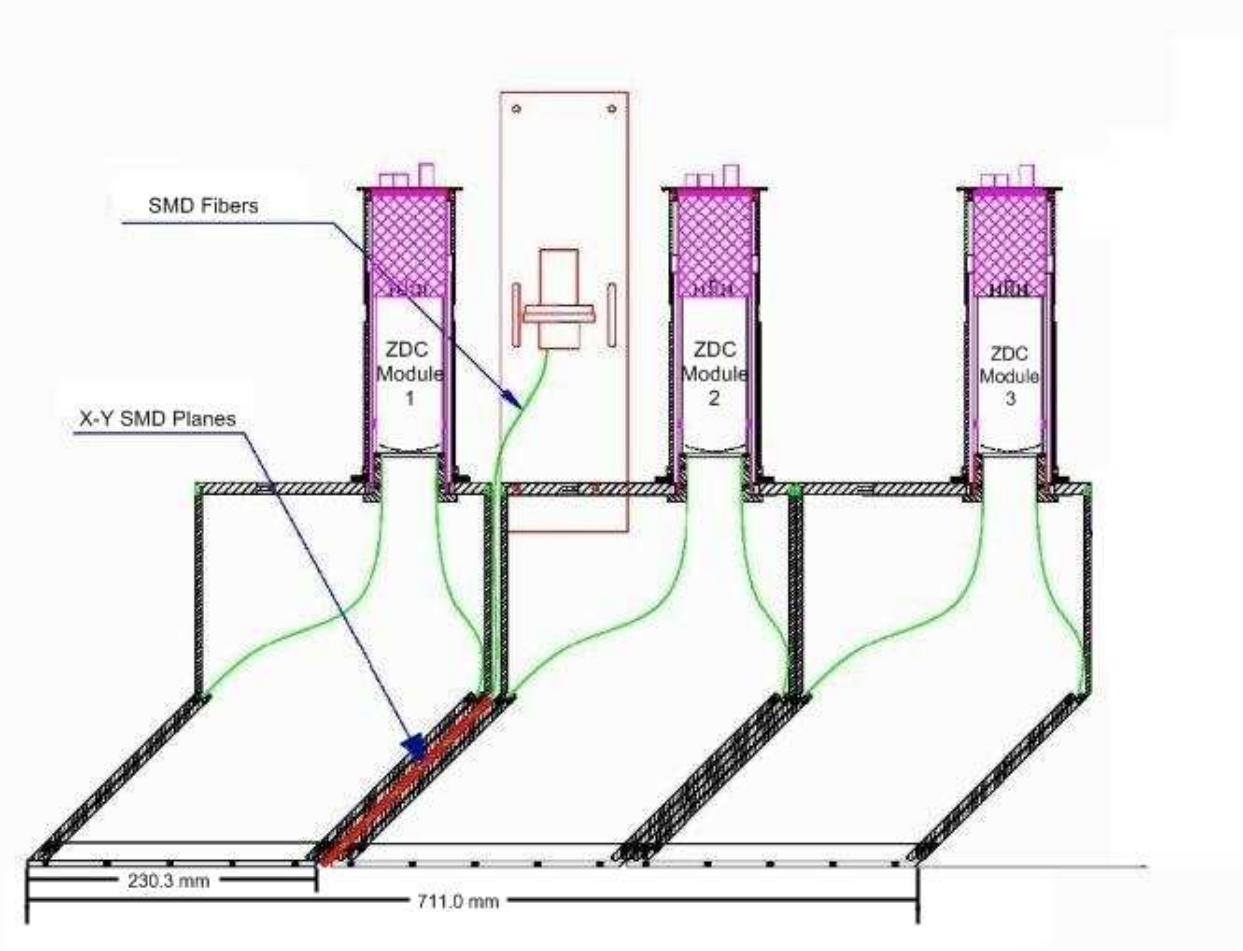

FIG. 2: Schematic of a Zero Degree Calorimeter. Each ZDC is composed of three identical modules tilted at a 45° angle to the beam, and is designed to contain an entire particle shower. The Shower Maximum Detectors (SMDs) are located between the first and second ZDC modules.

The ZDC is a Cherenkov-light sampling calorimeter, which provides the smallest shower-containment radius and maximum geometrical uniformity for detector response. The Cherenkov light is produced by charged shower secondaries from initial neutral-particle interactions. The detector is most sensitive to charged particles that cross at the Cherenkov angle, or approximately 45° to the fiber axis. Particles not coming in at the Cherenkov angle

are suppressed. This design allows the calorimeter to trigger on collisions.

The ZDCs were initially built without transverse segmentation, because the spatial resolution of the neutral particles emitted in the fragmentation region contains limited information about the collision. The ZDCs were also designed to minimize the loss in energy resolution due to shower leakage, which can cause fluctuations in the measured shower energy, by including aproximately 5 interaction lengths of material in the three modules.

The ZDC was upgraded to include a Shower Maximum Detector (SMD), which is used to provide position information of the showers initiated by the neutral particles. The SMD [5] is a scintillator hodoscope located between the first and second ZDC modules, and is composed of 8 horizontal slats and 7 vertical slats. The construction of the SMD is identical to that of the SMD used in the STAR Endcap Electromagnetic Calorimeter, described in Ref. [6]. A vertical slat means that the slat is aligned with its long axis vertical, and thus provides information on the horizontal position of the shower. Likewise, the horizontal slat provides vertical shower position. Each hodoscope slat consists of several scintillator strips; there are 4 strips in each horizontal slat (32 total horizontal strips) and 3 strips per vertical slat (21 total vertical strips). Figure 3 shows the SMD slat arrangement for the vertical and horizontal planes.

An SMD plane is constructed from these scintillator strips, each having a triangular cross section. The cross section is approximately an isosceles triangle with an apex-to-base height of 7 mm and base width of 10 mm. Running axially through the center of each triangular strip is a 0.83-mm-diameter, wavelength-shifting fiber that collects and transports light from the scintillator. Individual triangular strips are wrapped with 50-μm-thick, aluminized mylar to optically isolate them from their neighbors. The wrapped scintillator strips are then epoxied between two sheets of G-10 to form a plane. A diagram of an SMD plane, using the triangular scintillation strips, is shown in Figure 4. The overall hodoscope dimensions are approximately 18 cm (length) $\times$ 11 cm (width) $\times$ 2 cm (thick). The total 2-cm thickness of the SMD planes includes both scintillator and G-10 sheets. In addition, 21 strips combined have a width of 11.0 cm and 32 strips combined have a width of 16.5 cm.

The fiber from each strip is then routed to a 16-channel, segmented, multi-anode photomultiplier tube with a conventional resistive base. A channel measures light from each slat, and each channel connects to an ADC for pulse height analysis. The sixteenth channel from the phototube is a summed output, which is not used in this analysis. A shower produced

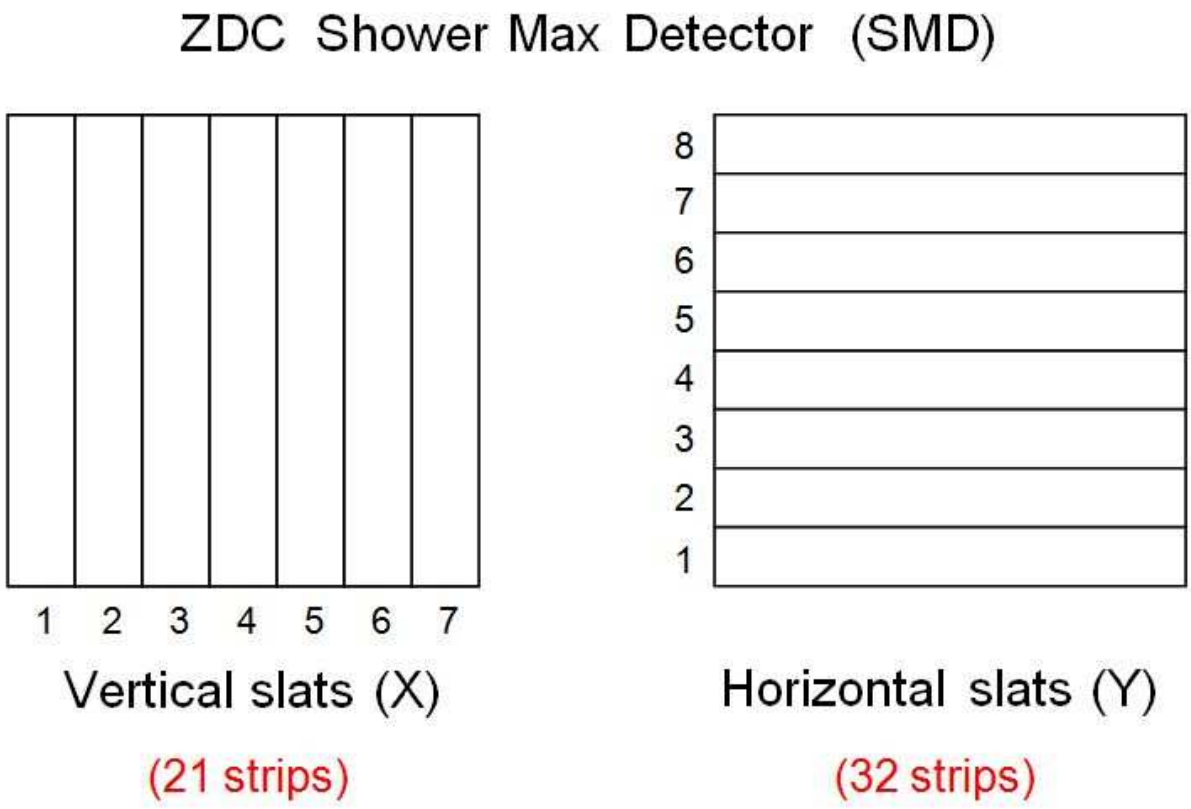

FIG. 3: Diagram of the arrangement of ZDC SMD slats. The SMD is composed of 8 horizontal and 7 vertical slats. Each vertical slat is composed of 3 strips (21 total vertical strips) and each horizontal slat has 4 strips (32 total horizontal strips).

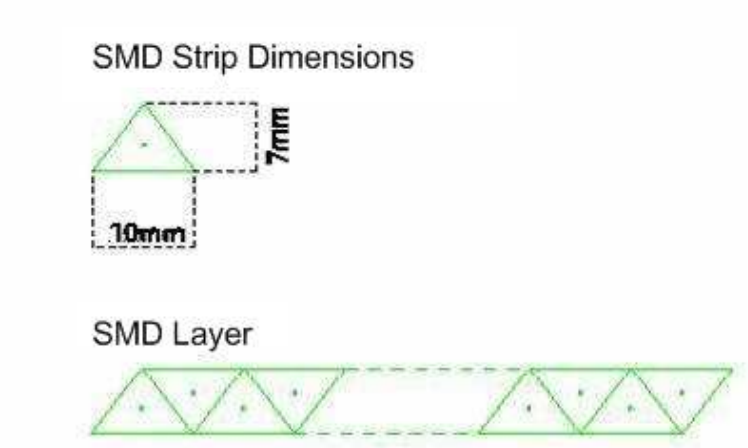

FIG. 4: Diagram of ZDC SMD strips. The dimensions of the cross section of each triangular SMD strip is shown, along with a group of these strips forming a plane.

by a neutral particle in the ZDC deposits light in more than one slat in each of the two layers of the SMD.

III. DATA ANALYSIS

Three dedicated STAR test runs of the ZDC SMD were taken on April 24, 2004 from about 2–3 AM EDT during fill number 5170. The data analyzed here were from runs 5115004, 5115007, and 5115008, with 4 million total events. Furthermore, the runs correspond to proton-proton interactions at $\sqrt{s} = 200$ GeV.

A. Pedestal and Gain Correction

Figure 5 shows a two-dimensional histogram of the ZDC SMD slat index versus the raw ADC value for each channel. Note that slat indices 1-7 represent the east ZDC that measure the SMD in the vertical direction, indices 9-16 the east ZDC in the horizontal, indices 17-23 the west ZDC in the vertical, and indices 25-32 the west ZDC in the horizontal.

In order to obtain valid energy measurements with the SMD, the raw ADC values must be corrected for pedestal and gain variations. A typical raw ADC spectrum from a ZDC SMD channel has a nonzero minimum value (pedestal), which is a normal design for an ADC with high sensitivity. The raw ADC spectrum for a channel must first be pedestal subtracted. To achieve this, a Gaussian fit was used to determine the pedestal for each channel, and a typical pedestal width was 1–2 channels. Each ADC channel was then adjusted according to its pedestal.

Next, each SMD channel was corrected for ADC gain to make the energy response of the detector more uniform. The ADC spectrum for each channel displays a pedestal peak followed by a longer tail at larger ADC values, as shown in Fig. 6. The tail of the ADC spectrum was fitted with an exponential function starting a distance of five channels larger than the pedestal. It was assumed that the ADC tail should have the same behavior for all the SMD channels, if the response of the detector is uniform. The parameters from the exponential function were used to calculate a gain ratio, and each SMD channel was adjusted accordingly. The improvement in response is shown in Figure 7, a two-dimensional histogram of SMD slat index versus the pedestal-subtracted and gain-corrected ADC values,

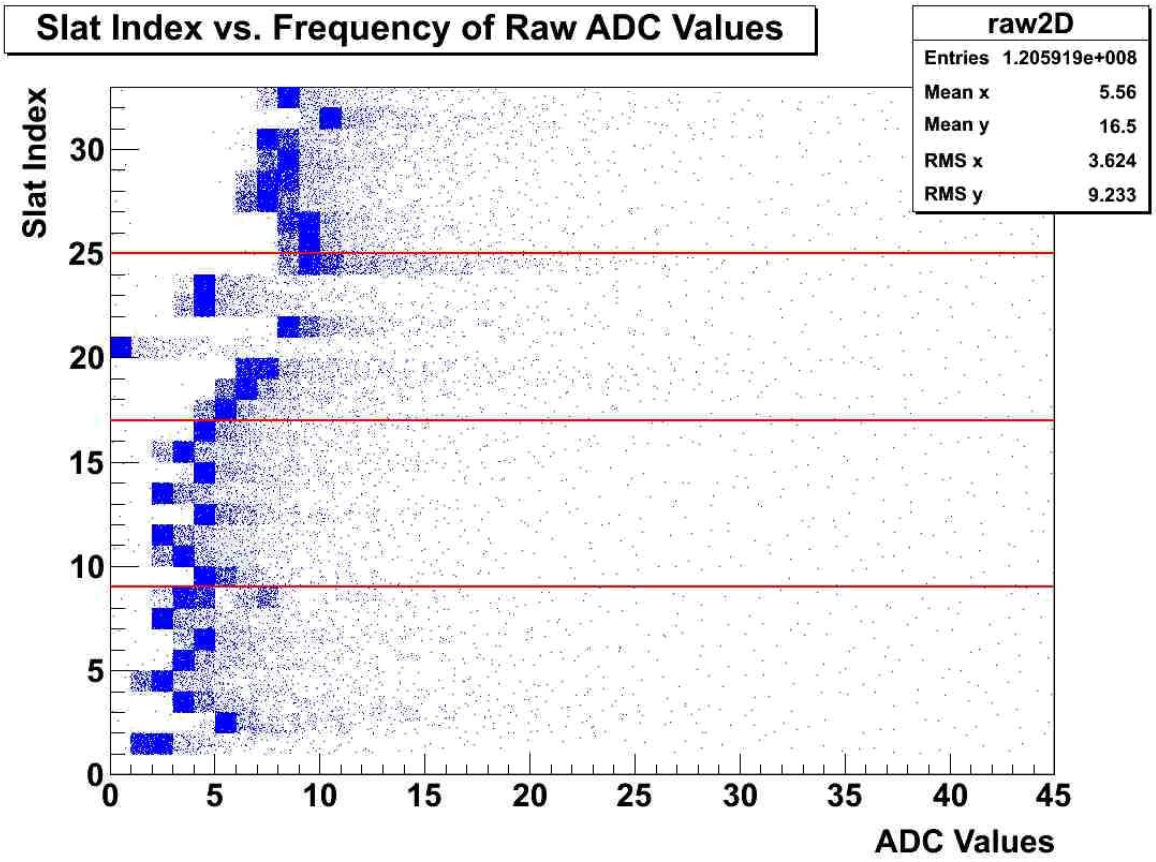

FIG. 5: Histogram of the SMD slat index versus its raw ADC value for all possible values. Note that before pedestal and gain corrections the ADC values are not aligned. Slat indices 1-7 represent the east ZDC vertical direction, 9-16 the east ZDC in the horizontal direction, 17-23 in the west ZDC vertical direction, and 25-32 in the west ZDC horizontal direction. Information from slat indices 8 and 24 are not used in this analysis.

as compared to the raw values shown in Figure 5. Note that in Fig. 7 some channels display binning effects; for example, when the gain has a value of two, every other bin would be empty.

Finally, after pedestal and gain corrections, a minimum ADC value was implemented. Good hits in the detector were defined as when the ADC value exceeded a threshold of at least 6 channels. Figure 8 again shows the slat index versus pedestal-subtracted and gain-corrected ADC values with a cut on ADC threshold. These ADC values are then counted as good hits.

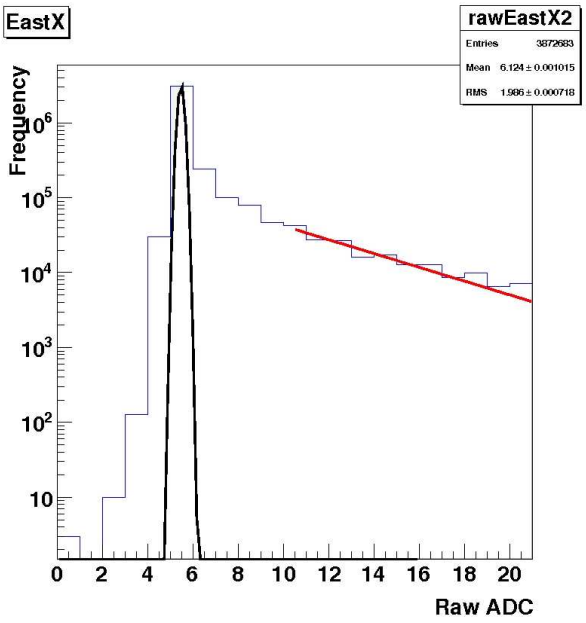

FIG. 6: Logarithmic plot of a single ADC channel. Fits were made of the large peak to determine the pedestal and the higher-energy tail for the gain.

B. Number of Hits vs. Slat Number

Figure 9a displays the number of good hits in the east ZDC horizontal direction (East X) versus slat number, and Figure 9b shows the number of good hits in the east ZDC vertical direction (East Y) versus slat number for all events. In the same manner, Figure 9c shows the number of good hits in the west ZDC horizontal direction (West X) versus slat number, and Figure 9d shows the number of good hits in the west ZDC vertical direction (West Y) for all events. It can be observed that the histograms are generally not symmetric about the middle.

C. X vs. Y Correlation

Figures 10a and 10b show plots of the largest (maximum) ADC value in the X direction vs. the largest ADC value in the Y direction for the east and west ZDC, respectively. In other words, the maximum ADC value in X and the maximum ADC value in Y for each event is plotted as a point, but only for both X and Y values above the threshold (a good hit)

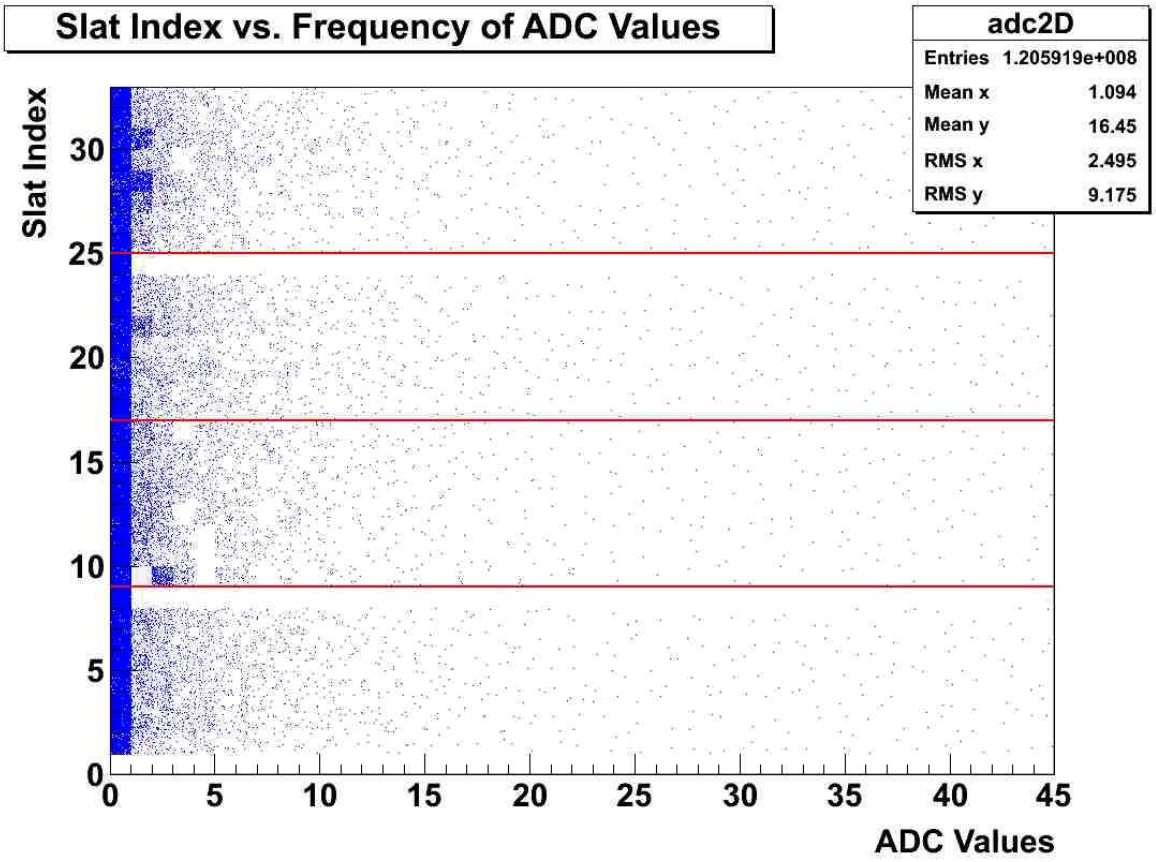

FIG. 7: Histogram of the SMD slat index versus corrected ADC value. The same slat index designations are used as those in Fig. 5. Note that slat indices 8 and 24 are not used by the SMD, and the ADC distributions in some channels are not smooth like Fig. 5 due to binning effects.

for a given ZDC. It is possible to see events with both an east and west ZDC hit. These plots show a band close to a 45° angle, which indicate similar ADC values in both planes. The ADC values should be similar since the X and Y strips are recording the same particle(s). The values may not be exactly the same since a hit is not always contained within one strip and energy can be lost in the shower. In addition, the response of the X and Y strips will not be the same due to different types and energies of particles. For example, the axes of the Y strips are approximately perpendicular to incoming neutrons, and there will be little sensitivity to Cherenkov light emitted by fast-moving charged particles in the scintillator. On the other hand, the axes of the X strips are 45° to the incoming neutrons, and thus they are much more sensitive to emitted Cherenkov light. Furthermore, the coupling of the scintillator light to the readout fibers for the X and Y strips may differ for the same reason.

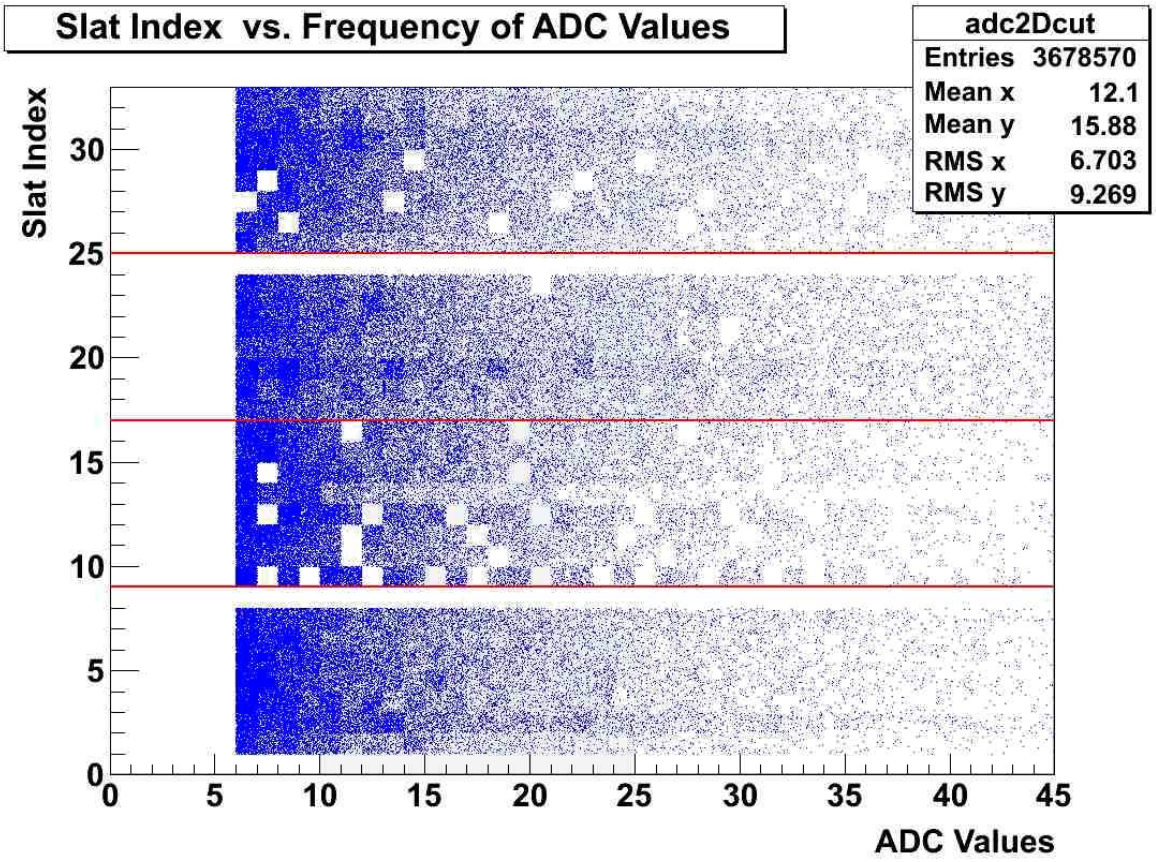

FIG. 8: Plot of the SMD slat index versus corrected ADC value. A minimum threshold cut was implemented, and the resulting values are considered as good hits. The same slat index designations are used as those in Fig. 5 and Fig. 7. The ADC distributions in some channels are not smooth due to binning effects.

D. Beam Bunch Spin Pattern

In order to calculate the asymmetries needed to make the ZDC into a useful polarimeter, the bunch spin pattern for a fill must be known. The bunch spin pattern was determined for fill 5170 during the ZDC SMD special runs by examining data from the number of events per bunch crossing in the ZDC and the raw bunch spin pattern. Figure 11 shows both the raw bunch spin pattern [7] and after correction from data analysis.

Figure 12 is the reference histogram showing the ZDC number of events per bunch crossing (bx7) for a subset of the full data sample. It can be seen that there are blanks with few or no particles for bunches 107 and 109, and all even bunch numbers 2–120, due to those bunches not being filled. Bunch numbers 32–40 and 113–119 are blank due to the accelerator

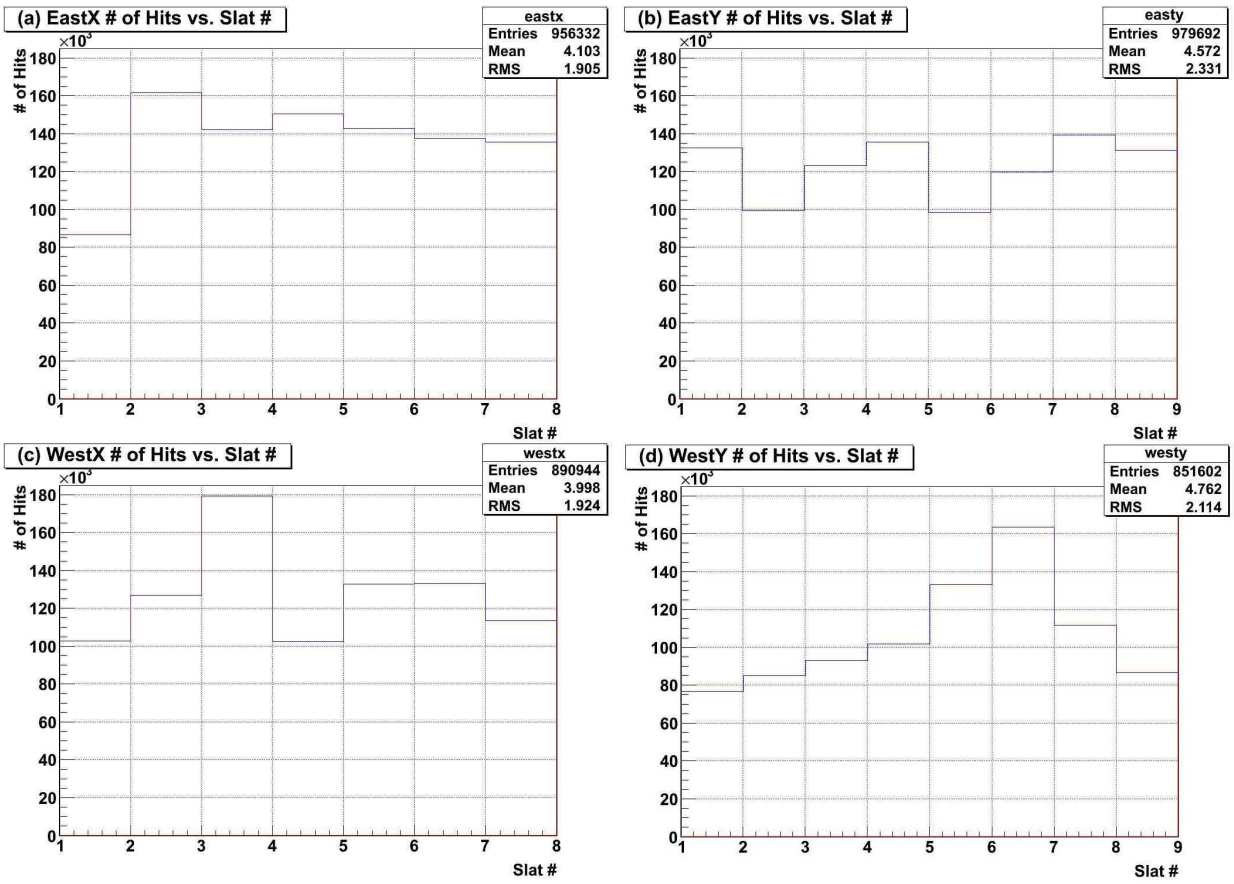

FIG. 9: Plots of the number of good hits vs. slat number. In the ZDC horizontal direction there are only 7 vertical slats.

abort gap. All of these blanks directly relate to the corrected bunch spin pattern. Nonzero ADC values are seen when both beam bunches are filled (+ +, - -). Moreover, there are no + - and - + states for this spin pattern because they were not included in the accelerator fill. It is important to note that despite the omission of the polarization states + - and - + during this fill, a physics asymmetry can still be calculated, as described in detail in the next section.

IV. RESULTS

A. Square Root Asymmetries with Two Spin States

The data were analyzed to give asymmetries with some simplifying assumptions using the "square root asymmetry" formulae. It will be assumed that the solid angle for event

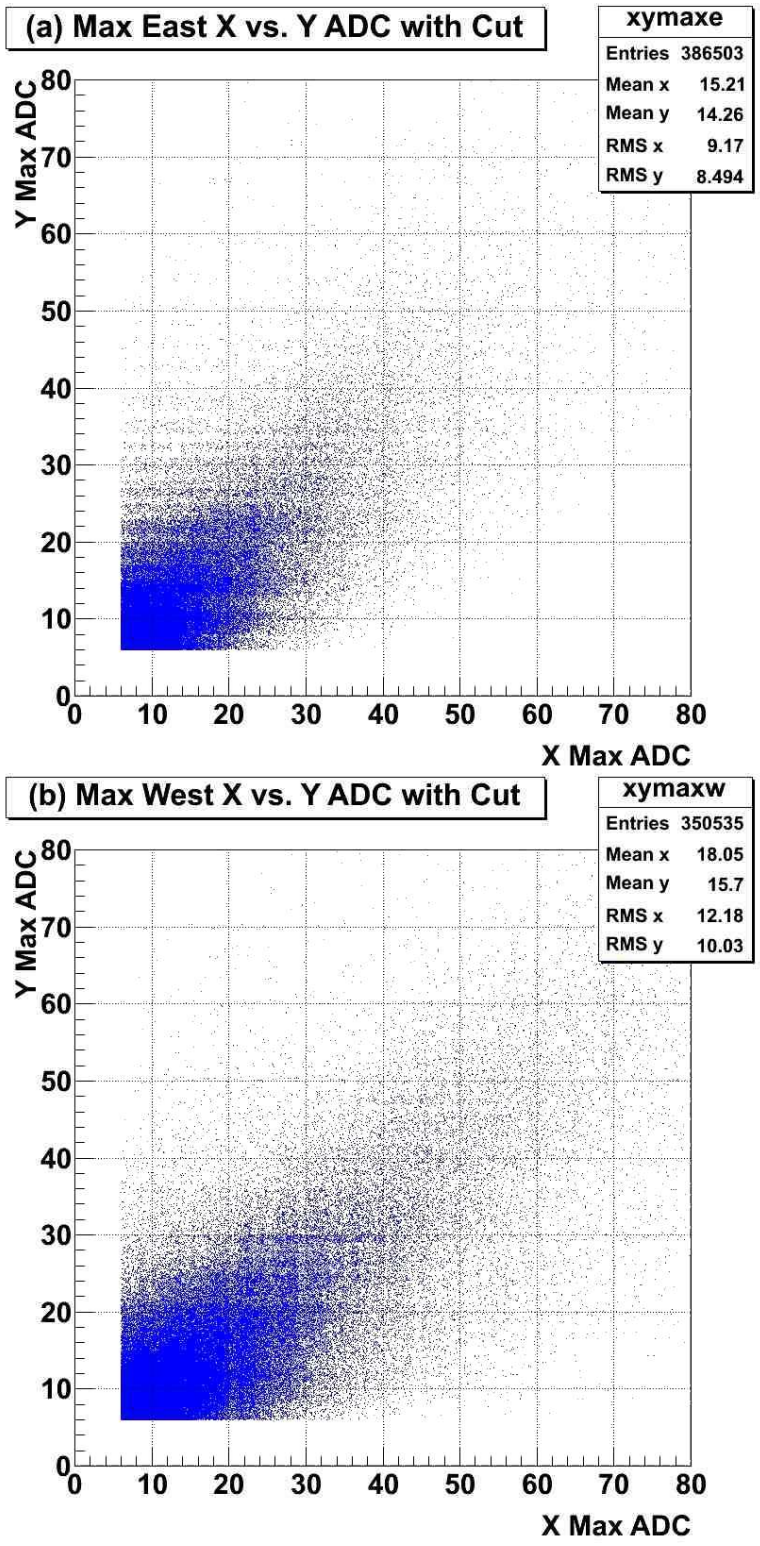

FIG. 10: Plots of (a) east and (b) west largest ADC value in the X direction vs. largest ADC value in the Y direction. The plot is close to a 45° angle. The ADC values should be similar because the X and Y strips are recording the same hit, though the values may not be exactly the same.

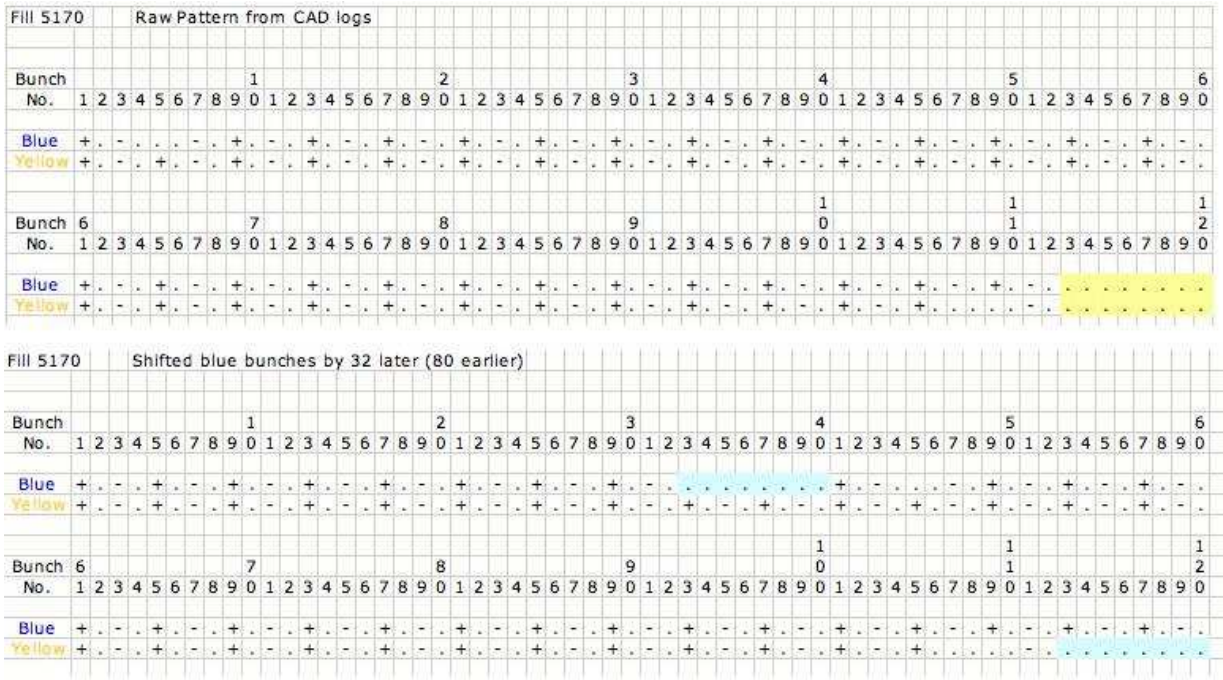

FIG. 11: Table of Raw and Corrected Bunch Spin Patterns. Note that some bunches contain blanks (32-40, 107, 109, 113-119, and evens 2-120), corresponding to the pattern from the accelerator fill.

detection is independent of spin state, and that the cross section does not vary significantly across the detector. Then for (approximately) symmetric sets of detectors on opposite sides of the beam (L = left, R = right), the number of counts recorded in some time for idealized east detectors will be

$$\begin{aligned}
N_{Le}^{\uparrow\uparrow} &= N_0\,\mathcal{L}^{\uparrow\uparrow}\,d\Omega_{Le}\,(1 + P_Y^{\uparrow}\,A_{Lfe} - P_B^{\uparrow}\,A_{Lbe} + P_Y^{\uparrow}\,P_B^{\uparrow}\,A_{NN,Le}) \\
N_{Le}^{\downarrow\downarrow} &= N_0\,\mathcal{L}^{\downarrow\downarrow}\,d\Omega_{Le}\,(1 - P_Y^{\downarrow}\,A_{Lfe} + P_B^{\downarrow}\,A_{Lbe} + P_Y^{\downarrow}\,P_B^{\downarrow}\,A_{NN,Le}) \\
N_{Re}^{\uparrow\uparrow} &= N_0\,\mathcal{L}^{\uparrow\uparrow}\,d\Omega_{Re}\,(1 - P_Y^{\uparrow}\,A_{Rfe} + P_B^{\uparrow}\,A_{Rbe} + P_Y^{\uparrow}\,P_B^{\uparrow}\,A_{NN,Re}) \\
N_{Re}^{\downarrow\downarrow} &= N_0\,\mathcal{L}^{\downarrow\downarrow}\,d\Omega_{Re}\,(1 + P_Y^{\downarrow}\,A_{Rfe} - P_B^{\downarrow}\,A_{Rbe} + P_Y^{\downarrow}\,P_B^{\downarrow}\,A_{NN,Re}),
\end{aligned}$$

where the integrated beam intensities are $\mathcal{L}^{\uparrow\uparrow}$ and $\mathcal{L}^{\downarrow\downarrow}$ for beam polarization directions up ($\uparrow$) and down ($\downarrow$), respectively. The analyzing powers for the L and R detectors are A_{Lfe} and A_{Rfe} for forward scattering by the yellow beam, and are A_{Lbe} and A_{Rbe} for backward scattering by the blue beam, respectively, and A_{NN} is the two-spin physics asymmetry. The products of solid angle and efficiency are $d\Omega_{Le}$ and $d\Omega_{Re}$. A normalization factor, N_0, is dependent on running time, cross section, etc. The blue and yellow beam polarizations are P_B and P_Y, and the L and R refer to left and right as viewed by the outgoing yellow beam

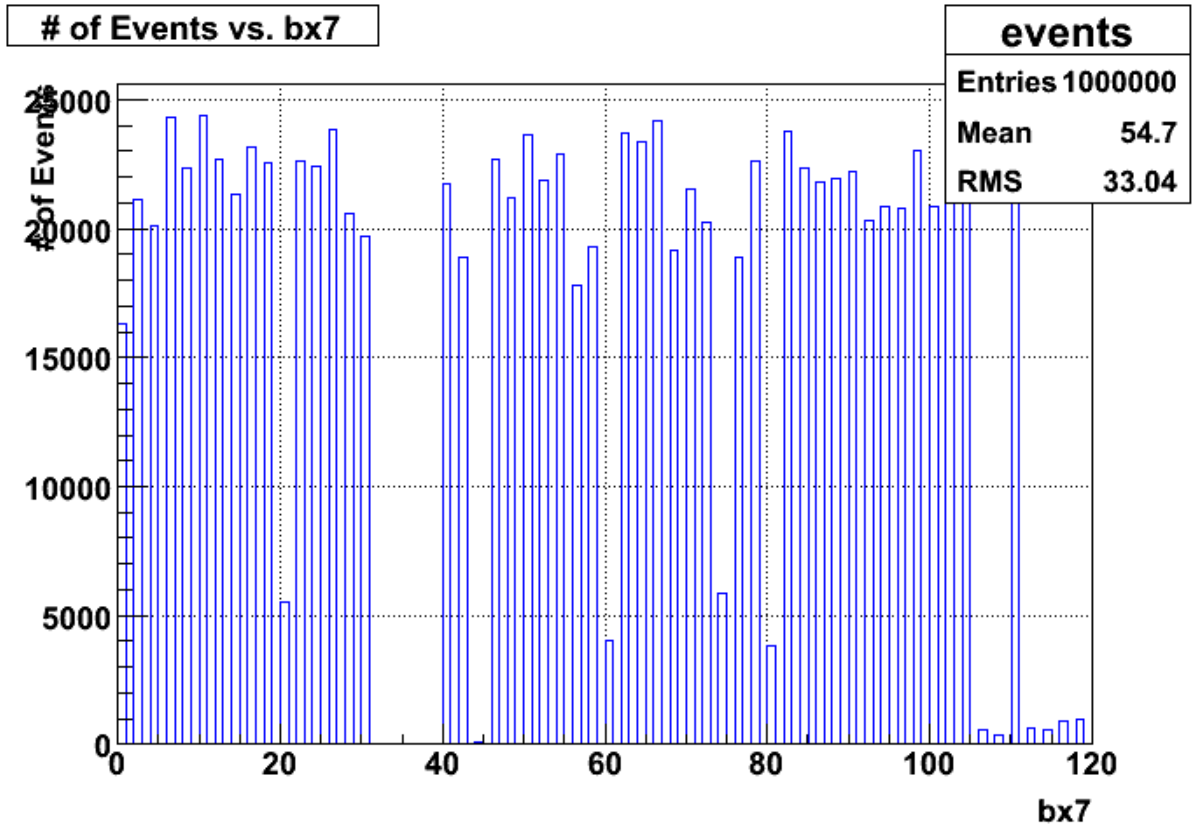

FIG. 12: Plot of the number of events in the ZDC per bunch crossing (bx7). The bunches with blanks (32-40, 107, 109, 113-119, and evens 2-120) correspond to the bunches with blanks from the corrected spin pattern displayed in Fig. 11.

in the east detectors; these are right and left as viewed by the outgoing blue beam, and hence the difference in sign for the terms with A_b.

Three square root asymmetries can be formed: a luminosity (ϵ^e_{lum}), a physics (ϵ^e_{phys}), and a geometrical (ϵ^e_{geom}) asymmetry. The "luminosity asymmetry" is defined as

$$\begin{aligned} \epsilon^e_{lum} &= \frac{\sqrt{N^{\uparrow\uparrow}_{Le}\,N^{\uparrow\uparrow}_{Re}} - \sqrt{N^{\downarrow\downarrow}_{Le}\,N^{\downarrow\downarrow}_{Re}}}{\sqrt{N^{\uparrow\uparrow}_{Le}\,N^{\uparrow\uparrow}_{Re}} + \sqrt{N^{\downarrow\downarrow}_{Le}\,N^{\downarrow\downarrow}_{Re}}} \\ &= \epsilon_{\mathcal{L}} + [P_Y\,A_{fe}\,\epsilon_{Afe} - P_B\,A_{be}\,\epsilon_{Abe} + P_Y\,P_B\,A_{NN,e}\,(\epsilon_{PY} + \epsilon_{PB})] + h.o.t., \end{aligned} \tag{1}$$

where the higher-order terms ("h.o.t.") are third order in small quantities, ($P_Y\,A_{fe}$, $P_B\,A_{be}$, $P_Y\,P_B\,A_{NN,e}$, $\epsilon_{\mathcal{L}}$, ϵ_{PY}, ϵ_{PB}, ϵ_{Afe}, ϵ_{Abe}, and $\epsilon_{ANN,e}$) described below. Note ϵ_{lum} is primarily

sensitive to $\epsilon_{\mathcal{L}}$, which is

$$\epsilon_{\mathcal{L}} \;=\; \frac{\mathcal{L}^{\uparrow\uparrow} \,-\, \mathcal{L}^{\downarrow\downarrow}}{\mathcal{L}^{\uparrow\uparrow} \,+\, \mathcal{L}^{\downarrow\downarrow}}, \tag{2}$$

since all other terms are second order or higher in small quantities.

The "physics asymmetry" can be determined from the formula

$$\begin{aligned} \epsilon^{e}_{phys} \;&=\; \frac{\sqrt{N^{\uparrow\uparrow}_{Le}\, N^{\downarrow\downarrow}_{Re}} \,-\, \sqrt{N^{\downarrow\downarrow}_{Le}\, N^{\uparrow\uparrow}_{Re}}}{\sqrt{N^{\uparrow\uparrow}_{Le}\, N^{\downarrow\downarrow}_{Re}} \,+\, \sqrt{N^{\downarrow\downarrow}_{Le}\, N^{\uparrow\uparrow}_{Re}}} \\ &=\; \frac{P_Y\, A_{fe} \,-\, P_B\, A_{be}}{1 \,+\, P_Y\, P_B\, A_{NN,e}} \;+\; h.o.t. \end{aligned} \tag{3}$$

where the h.o.t. are fourth order in terms of the all the same small quantities as ϵ^{e}_{lum} with the exception of $\epsilon_{\mathcal{L}}$. The average beam polarizations are

$$\begin{aligned} P_Y \;&=\; \frac{1}{2}(P_Y^{\uparrow} \,+\, P_Y^{\downarrow}) \\ P_B \;&=\; \frac{1}{2}(P_B^{\uparrow} \,+\, P_B^{\downarrow}) \end{aligned}$$

and the average analyzing powers and two spin correlation parameter are

$$\begin{aligned} A_{fe} \;&=\; \frac{1}{2}(A_{Lfe} \,+\, A_{Rfe}) \\ A_{be} \;&=\; \frac{1}{2}(A_{Lbe} \,+\, A_{Rbe}) \\ A_{NN,e} \;&=\; \frac{1}{2}(A_{NN,Le} \,+\, A_{NN,Re}). \end{aligned}$$

Equation (3) was derived under the assumption that only two of the usual four spin states were available, as is the case for these data. An unfortunate consequence is the presence of the two-spin observable A_{NN} in the expression, but remarkably the differences in beam polarizations (up, down) or analyzing powers (left, right) do not enter into the asymmetry calculation except as much higher-order corrections.

The "geometrical asymmetry" is defined as

$$\begin{aligned} \epsilon^{e}_{geom} \;&=\; \frac{\sqrt{N^{\uparrow\uparrow}_{Le}\, N^{\downarrow\downarrow}_{Le}} \,-\, \sqrt{N^{\uparrow\uparrow}_{Re}\, N^{\downarrow\downarrow}_{Re}}}{\sqrt{N^{\uparrow\uparrow}_{Le}\, N^{\downarrow\downarrow}_{Le}} \,+\, \sqrt{N^{\uparrow\uparrow}_{Re}\, N^{\downarrow\downarrow}_{Re}}} \\ &=\; \epsilon_{d\Omega e} \;+\; [P_Y\, A_{fe}\, \epsilon_{PY} \;-\; P_B\, A_{be}\, \epsilon_{PB} \;+\; P_Y\, P_B\, A_{NN,e}\, \epsilon_{ANN,e}] \;+\; h.o.t., \end{aligned} \tag{4}$$

where the h.o.t. are again third order in the same quantities as ϵ^e_{lum}, except $\epsilon_{\mathcal{L}}$ is not present and $\epsilon_{d\Omega}$ is present. The remaining small quantities are defined as

$$\begin{aligned}
\epsilon_{Afe} &= \frac{A_{Lfe} - A_{Rfe}}{A_{Lfe} + A_{Rfe}} \\
\epsilon_{Abe} &= \frac{A_{Lbe} - A_{Rbe}}{A_{Lbe} + A_{Rbe}} \\
\epsilon_{ANN,e} &= \frac{A_{NN,Le} - A_{NN,Re}}{A_{NN,Le} + A_{NN,Re}} \\
\epsilon_{d\Omega e} &= \frac{d\Omega_{Le} - d\Omega_{Re}}{d\Omega_{Le} + d\Omega_{Re}} \\
\epsilon_{PY} &= \frac{P_Y^{\uparrow} - P_Y^{\downarrow}}{P_Y^{\uparrow} + P_Y^{\downarrow}} \\
\epsilon_{PB} &= \frac{P_B^{\uparrow} - P_B^{\downarrow}}{P_B^{\uparrow} + P_B^{\downarrow}}.
\end{aligned}$$

The luminosity asymmetries from east and west detectors, and from both left-right and up-down sets of slats, are all expected to be equal, as the second- and higher-order terms are probably quite small. The geometrical asymmetries will not be particularly useful, as they record information primarily about the detectors' efficiency and solid angle.

The up-down physics asymmetries should be consistent with zero, since the beam polarization direction during this run period was vertical. The east and west analyzing powers and two spin correlation parameters, $A_{NN,e}$ and $A_{NN,w}$, are expected to be equal since the construction of the detectors was the same for the two ZDCs. Finally, the yellow and blue beam polarizations are typically nearly equal. Thus, the left-right physics asymmetries are expected to be equal from the east and west detectors. Note for the west detectors,

$$\begin{aligned}
\epsilon^w_{phys} &= \frac{\sqrt{N^{\uparrow\uparrow}_{Lw}\, N^{\downarrow\downarrow}_{Rw}} - \sqrt{N^{\downarrow\downarrow}_{Lw}\, N^{\uparrow\uparrow}_{Rw}}}{\sqrt{N^{\uparrow\uparrow}_{Lw}\, N^{\downarrow\downarrow}_{Rw}} + \sqrt{N^{\downarrow\downarrow}_{Lw}\, N^{\uparrow\uparrow}_{Rw}}} \\
&= \frac{P_B\, A_{fw} - P_Y\, A_{bw}}{1 + P_Y\, P_B\, A_{NN,w}} + h.o.t.
\end{aligned} \tag{5}$$

In this paper, slat-by-slat asymmetries can also be calculated. For completeness, the expressions for these quantities will be included here. For a slat i to the left of the beam, on the east side of the STAR detector,

$$\begin{aligned}
N^{\uparrow\uparrow}_{Le,i} &= N_0 \mathcal{L}^{\uparrow\uparrow} d\Omega_{Le,i}(1 + P_Y^{\uparrow} A_{Lfe,i} - P_B^{\uparrow} A_{Lbe,i} + P_Y^{\uparrow} P_B^{\uparrow} A_{NN,Lei}) \\
N^{\downarrow\downarrow}_{Le,i} &= N_0 \mathcal{L}^{\downarrow\downarrow} d\Omega_{Le,i}(1 - P_Y^{\downarrow} A_{Lfe,i} + P_B^{\downarrow} A_{Lbe,i} + P_Y^{\downarrow} P_B^{\downarrow} A_{NN,Lei}).
\end{aligned}$$

Then the slat-by-slat physics asymmetry is defined as

$$\begin{aligned}
\epsilon^{e}_{phys,i} &= \frac{N^{\uparrow\uparrow}_{Le,i} \; - \; \mathcal{R} N^{\downarrow\downarrow}_{Le,i}}{N^{\uparrow\uparrow}_{Le,i} \; + \; \mathcal{R} N^{\downarrow\downarrow}_{Le,i}} \\
&= \frac{P_Y A_{Lf,i} \; - \; P_B A_{Lb,i}}{1 \; + \; P_Y P_B A_{NN,Li}} \; + \; h.o.t. \\
&\simeq \frac{N^{\uparrow\uparrow}_{Le,i}/\mathcal{L}^{\uparrow\uparrow} \; - N^{\downarrow\downarrow}_{Le,i}/\mathcal{L}^{\downarrow\downarrow}}{N^{\uparrow\uparrow}_{Le,i}/\mathcal{L}^{\uparrow\uparrow} \; + \; N^{\downarrow\downarrow}_{Le,i}/\mathcal{L}^{\downarrow\downarrow}},
\end{aligned} \tag{6}$$

where the quantities are defined in analogy to earlier values, and

$$\begin{aligned}
\mathcal{R} &= \frac{1 \; + \; < \epsilon_{lum} >}{1 \; - \; < \epsilon_{lum} >} \\
&\simeq \frac{\mathcal{L}^{\uparrow\uparrow}}{\mathcal{L}^{\downarrow\downarrow}}.
\end{aligned}$$

The higher-order terms in the equation above are second order in small quantities, rather than fourth order in the square root asymmetry.

B. Numerical Results

Table I displays all of the luminosity, geometrical, and physics asymmetries for the East and West SMDs. Up-Down asymmetries were calculated by combining slats 1, 2, 3, and 4 to make the down group, and combining slats 5, 6, 7, and 8 to make the up group. Left-Right asymmetries were calculated by combining slats 1, 2, and 3 to make the left group, and combining slats 5, 6, and 7 to make the right group. No more than one hit per event was used in calculating the following results. For each event, only the maximum X and Y slats above the threshold were counted as a hit for east and west, respectively. Several conclusions can be drawn from the numerical results and are summarized below.

	ϵ_{lum}	ϵ_{geom}	ϵ_{phys}
East Left-Right	-0.0970 ± 0.0018	-0.0302 ± 0.0018	0.0130 ± 0.0018
East Up-Down	-0.0965 ± 0.0016	-0.0258 ± 0.0016	-0.0019 ± 0.0016
West Left-Right	-0.0934 ± 0.0018	0.0828 ± 0.0018	0.0138 ± 0.0018
West Up-Down	-0.0930 ± 0.0017	0.1531 ± 0.0017	0.0023 ± 0.0017

TABLE I: Experimental values of the luminosity, geometrical, and physics asymmetries.

The luminosity asymmetries for east and west detectors were as expected: the same values were found within experimental uncertainties. Both left-right and up-down luminosity asymmetries are all equal, since the second- and higher-order terms are most likely rather small. The large magnitudes for these asymmetries come from the differences in the numbers of events in each of the ++ polarization bunches compared to the - - bunches; see Fig. 12.

Nonzero geometrical asymmetries occur when there is an inefficient slat on one side compared to the other. This type of asymmetry is directly related to the number of hits versus slat number histograms (Figures 9a-d), where the shapes of the curves are generally not symmetric about the middle. The geometrical asymmetries are not extremely useful for this analysis, although they do give some indication of how well the detector worked by recording information about efficiency and solid angle. In the future, this information could be used to better align the position of the ZDC detectors and match their output gains.

The physics asymmetries for the east and west detectors show values consistent with zero for the up-down asymmetries and a seven-sigma effect in the left-right asymmetries. The large left-right physics asymmetries from east and west are approximately equal because the yellow and blue beam polarizations, analyzing powers, and two-spin correlation parameters are about equal. In addition, the up-down physics asymmetries for east and west are consistent with zero because the beam polarization direction during the run period was vertical.

Figure 13 displays the physics asymmetries for each horizontal and vertical slat for both east and west ZDC. As is expected with transversely-polarized particles, the asymmetry values for both sets of horizontal slats are consistent with zero, and the patterns of asymmetries for the vertical slats are observed to be nearly the same, and to have a cosine dependence, passing through zero for the central slat.

As a final test, an angular distribution of the left-right physics asymmetry was made. Coincidental hits in both X and Y SMD planes for a given detector were assigned to bins according to an angle ϕ, which measures counterclockwise the angle from the vertical direction. This ϕ angle definition is shown in Figure 14 and the binning map of hits grouped by ϕ is given in Figure 15. Group one is $\frac{\pi}{2}$ rad, group three is roughly $\frac{\pi}{4}$ rad, group five is 0 rad, and group seven is approximately -$\frac{\pi}{4}$ rad. Note that groups three and seven consist of counters along the diagonal, but the widths of the X and Y bins are slightly different. In these cases, four Y strips physically inclined at 45° are not exactly equal to the width of

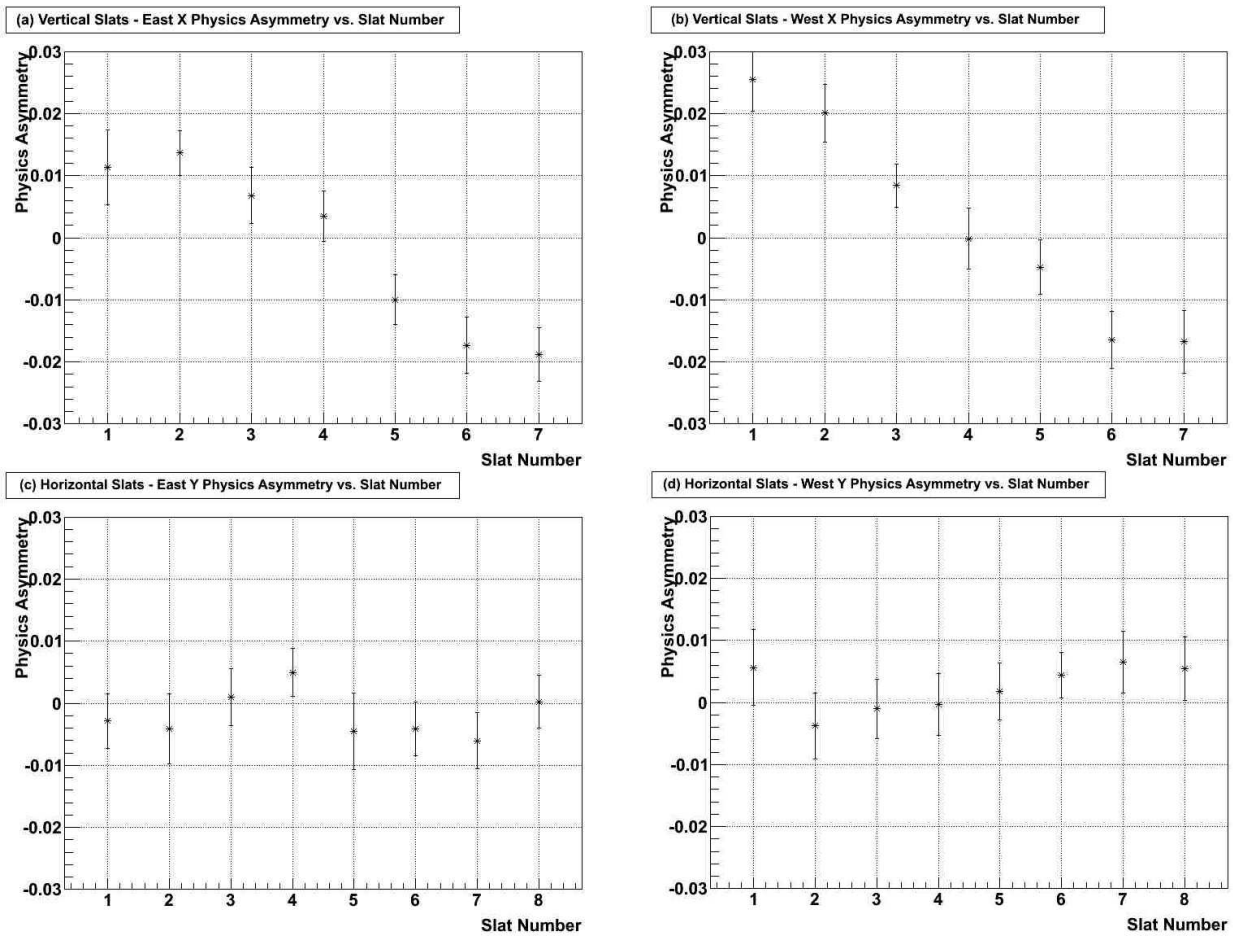

FIG. 13: Plots of calculated physics asymmetries for each detector slat. Asymmetries for the horizontal slats are consistent with zero, while the vertical-slat asymmetries are not.

three X strips.

The formula used for calculating the physics asymmetry is

$$\epsilon_{phys} = \frac{\sqrt{N_L^{\uparrow} N_R^{\downarrow}} - \sqrt{N_L^{\downarrow} N_R^{\uparrow}}}{\sqrt{N_L^{\uparrow} N_R^{\downarrow}} + \sqrt{N_L^{\downarrow} N_R^{\uparrow}}}, \tag{7}$$

where L and R refer to the bins on opposite sides of the SMD as shown in Figure 15. Figure 16 shows the physics asymmetry ϕ distribution for East and West. The function (p0)sin(ϕ) was applied as a fit, where p0 is a fit parameter representing the amplitude of the sine curve, and the results are also displayed in Figure 16. The left-right physics asymmetry is expected to be zero at $\phi = 0$ rad and have its maximum value at $\phi = \frac{\pi}{2}$ rad or $\phi = -\frac{\pi}{2}$ rad. This pattern is observed in Figure 16 and thus a sine curve can be seen in the asymmetry ϕ distribution.

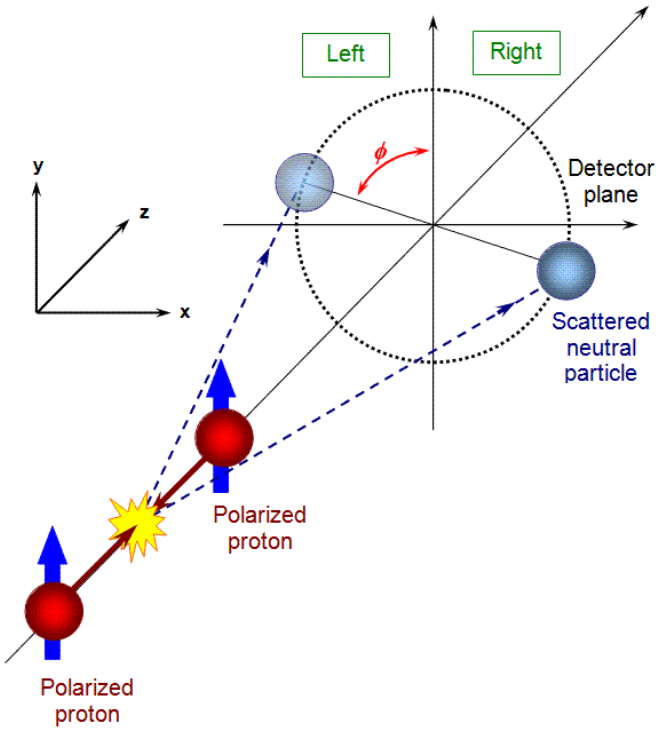

FIG. 14: Diagram of Single Transverse-Spin Asymmetry. The angle ϕ in the detector plane of hits is defined from the vertical direction, as shown. Figure is adapted from Ref. [8].

The approximate analyzing power of the ZDC SMDs for polarimetry can be estimated from the fitted value of p0 in Figure 16. With p0 $= 0.021 \pm 0.002$ and an approximate beam polarization of 0.26 ± 0.03 from Ref. [9], the analyzing power is then $A_N = 0.081 \pm 0.012$. This result is slightly larger than that quoted for the PHENIX ZDC SMD of $A_N = -0.066 \pm 0.006$ stated in Ref. [10]. Note that the A_N value derived from these measurements is actually the difference, $A_f - A_b$, from Eq. (3), whereas the PHENIX A_N result is A_f. An attempt failed to reconcile the difference in sign between these measurements and the one from PHENIX.

V. CONCLUSIONS

A careful analysis of SMD data from the ZDCs at STAR, taken in 2004 using transversely-polarized proton-proton collisions at $\sqrt{s} = 200$ GeV, has shown an approximately seven-sigma, left-right physics asymmetry. No corresponding up-down physics asymmetry was observed. An asymmetry due to luminosity was also calculated and found to be consistent for up-down, left-right, east and west data sets; a geometrical asymmetry was also calcu-

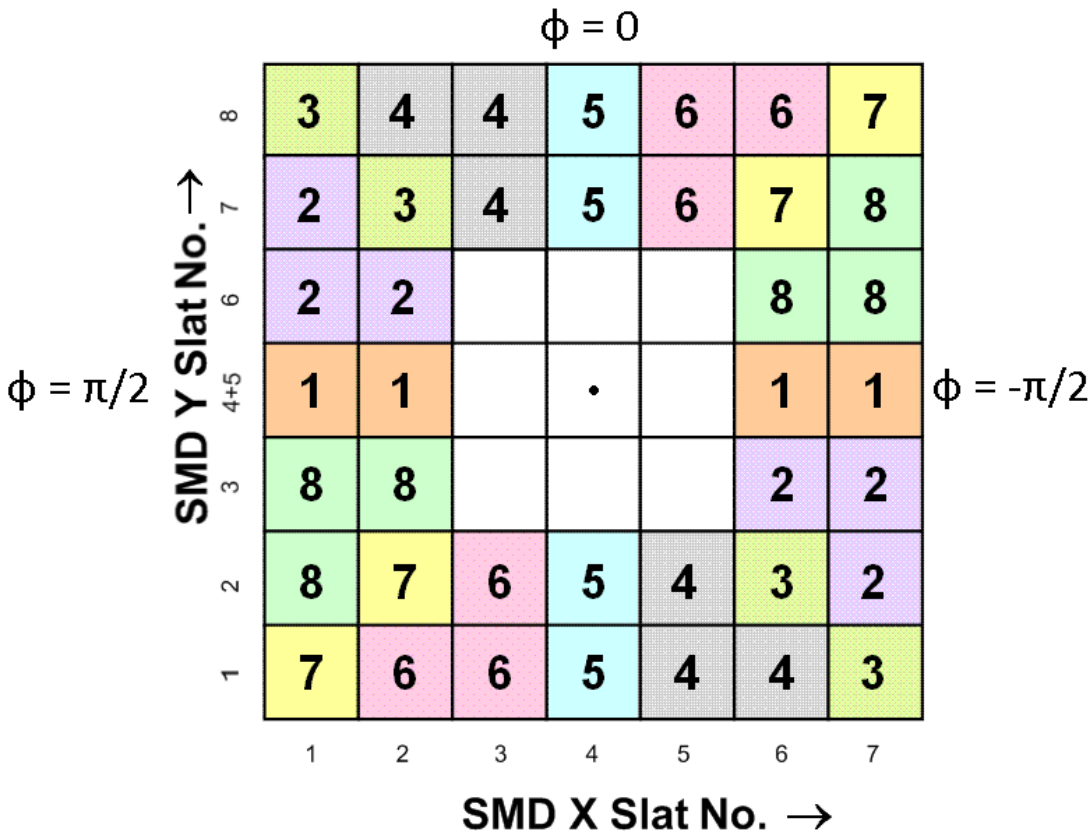

FIG. 15: Map of ZDC SMD bins used with the physics asymmetry ϕ distribution. Coincidental hits in the SMD X-Y planes were assigned to eight bins, further divided into left and right groups, according to the azimuthal angle ϕ.

lated. Finally, graphs of the physics asymmetry as a function of azimuthal angle indicate a sinusoidal pattern, as observed previously in other experiments. An analyzing power of $A_N = 0.081 \pm 0.012$ was calculated for this reaction. All of this evidence proves that the ZDC SMD can be used as a local polarimeter for STAR at $\sqrt{s} = 200$ GeV, and suggests strong potential for use at 500 GeV as well.

In future analyses, it will be productive to double-check these ZDC SMD results against corresponding BBC (Beam-Beam Counter) values. Furthermore, these results should be checked with all spin patterns, since only transverse + + and - - spin states were available during these runs. Data from longitudinally-polarized protons should be analyzed to determine physics asymmetries, and the ϕ distribution should be verified as zero. Ultimately, the same ZDC SMD analysis should be applied to polarized-proton beams at $\sqrt{s} = 500$ GeV.

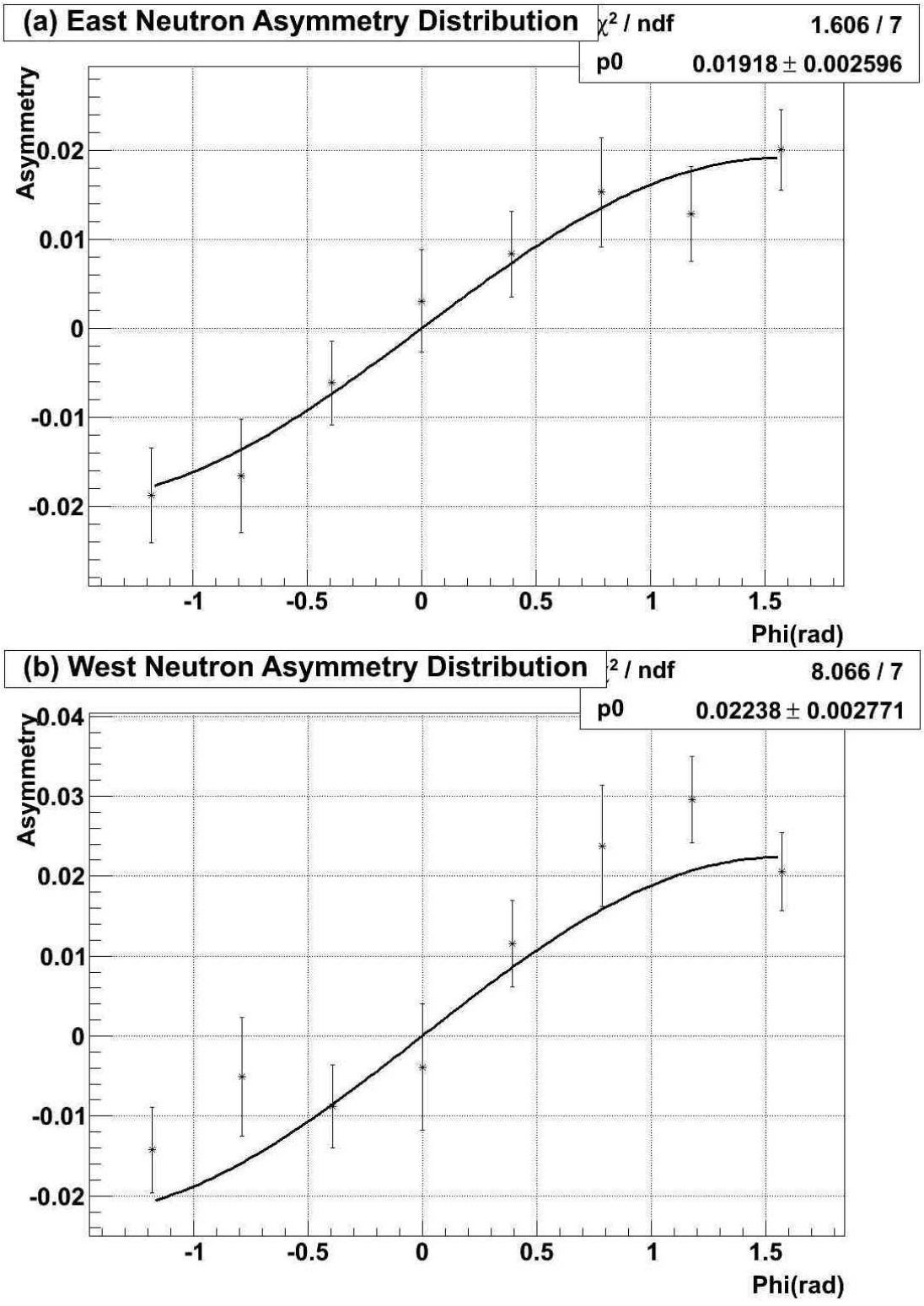

FIG. 16: Plot of (a) east and (b) west ZDC physics asymmetry ϕ distribution. Note that the left-right physics asymmetry is zero at $\phi = 0$ rad and has maximum values at $\phi = \frac{\pi}{2}$ or -$\frac{\pi}{2}$ rad. The fit is to a sine curve with an amplitude of p0.

VI. ACKNOWLEDGMENTS

The authors are grateful to Alice Bridgeman, Hank Crawford, Declan Keane, Spencer Klein, Mikhail Kopytine, Aihong Tang, Sergei Voloshin, Gang Wang, and Zhangbu Xu for making this analysis possible by upgrading the STAR ZDC with the Shower Maximum Detector. The authors also thank the staff of the Collider-Accelerator and Physics Departments at BNL for their diligent efforts. This work was supported in part by the United States Department of Energy, Office of Science, Division of Nuclear Physics under Contract No. DE-AC02-06CH11357 and Grant No. DE-FG02-88ER40416.

---

[1] J. Adams *et al.*, Phys. Rev. C**73**, 034903 (2006).

[2] Y. Fukao *et al.*, Phys. Lett. B**650**, 325 (2007).

[3] M. Togawa, in Proceedings of the 12th International Conference on Elastic and Diffractive Scattering - Forward Physics and QCD, DESY preprint DESY-PROC-2007-02 and arXiv:0712.3633 (2007) p 308.

[4] C. Adler *et al.*, Nucl. Instrum. Meth. A**470**, 488 (2001).

[5] H. Crawford *et al.*, STAR note SN-0448 (2003).

[6] C.E. Allgower *et al.*, Nucl. Instrum. Meth. A**499**, 740 (2003).

[7] H. Huang, private communication.

[8] K. Boyle, presented at PANIC 2005, Santa Fe, NM, 2005 (unpublished). Presentation slides are given in http://www.panic05.lanl.gov/abstracts/594/Boyle 594 panic05.ppt.

[9] M. Bai, presentation to the BNL C-AD Retreat; see http://www.agsrhichome.bnl.gov/AP /RHIC2004/Retreat/Bai-PpRun2004.ppt.

[10] M. Togawa, in AIP Conference Proceedings 915, Proceedings of the 17th International Spin Physics Symposium, edited by K. Imai, T. Murakami, N. Saito, and K. Tanida, (American Institute of Physics, Melville, NY, 2007), p. 689.